



Simulation model of Reactive Nitrogen Species in an Urban Atmosphere using a Deep Neural Network: RNDv1.0

Junsu Gil¹, Meehye Lee¹, Jeonghwan Kim², Gangwoong Lee², Joonyoung Ahn³, and Cheol-Hee Kim⁴

¹Department of Earth and Environmental Sciences, Korea University, Seoul, South Korea

²Department of Environmental Science, Hankuk University of Foreign Studies, Yongin, South Korea

³Climate and Air Quality Research Department, Air Quality Forecasting Center, National Institute of Environmental Research (NIER), Incheon, South Korea

⁴Department of Atmospheric Sciences, Pusan National University, Busan, South Korea

Correspondence: Meehye Lee (meehye@korea.ac.kr)

Received: 13 October 2021 – Discussion started: 10 December 2021

Revised: 29 June 2023 – Accepted: 8 August 2023 – Published: 13 September 2023

Abstract. Nitrous acid (HONO) plays an important role in the formation of ozone and fine aerosols in the urban atmosphere. In this study, a new simulation approach is presented to calculate the HONO mixing ratios using a deep neural technique based on measured variables. The Reactive Nitrogen Species using a Deep Neural Network (RND) simulation is implemented in Python. The first version of RND (RNDv1.0) is trained, validated, and tested with HONO measurement data obtained in Seoul, South Korea, from 2016 to 2021. RNDv1.0 is constructed using k -fold cross validation and evaluated with index of agreement, correlation coefficient, root mean squared error, and mean absolute error. The results show that RNDv1.0 adequately represents the main characteristics of the measured HONO, and it is thus proposed as a supplementary model for calculating the HONO mixing ratio in a polluted urban environment.

1 Introduction

Surface ozone (O_3) pollution has worsened over continental areas (Arnell et al., 2019; Monks et al., 2015; IPCC, 2014; Varotsos et al., 2013). Particularly, a warmer climate is expected to increase the surface O_3 concentrations and peak levels in polluted regions depending on its precursor levels (IPCC, 2023). As a short-lived climate pollutant (SLCP), O_3 interacts with the global temperature via positive feedback (Myhre et al., 2017; Shindell et al., 2013; Stevenson et al., 2013). Therefore, accurate predictions of the mixing ratios

and variations in the surface O_3 are essential. While operational models such as the Community Multiscale Air Quality (CMAQ) model have been widely used for this purpose, uncertainties still arise from poorly understood chemical mechanisms involving reactive nitrogen oxides (NO_y) and volatile organic compounds (VOCs), as well as the lack of their measurements (Cheng et al., 2022; Akimoto et al., 2019; Shareef et al., 2019; Canty et al., 2015; Mallet and Sportisse, 2006)

In the urban atmosphere, NO_y typically includes NO_x ($NO + NO_2$), HONO, HNO_3 , organic nitrates (e.g., PAN), NO_3 , N_2O_3 , and particulate NO_3^- . These species are produced and recycled through photochemical reactions until they are removed through wet or dry deposition (Li et al., 2020; Wang et al., 2020; Liebmann et al., 2018; Brown et al., 2017). NO_y plays an important role in critical environmental issues concerning the Earth's atmosphere from local air pollution to global climate change (Ge et al., 2019; Sun et al., 2011). The oxidation of NO to NO_2 and finally to HNO_3 is the backbone of the chemical mechanism producing ozone (O_3) and $PM_{2.5}$ (particulate matter with size $\leq 2.5 \mu m$), and it determines the oxidization capacity of the atmosphere. Recently, as O_3 has still increased even with decreasing NO_x emissions over many regions, including East Asia, interest in the heterogeneous reaction of NO_y , which is yet to be understood, has increased (Stadtler et al., 2018; Brown et al., 2017). Currently, the lack of measurements of individual NO_y species is hindering a comprehensive understanding of the heterogeneous reactions (Akimoto and Tanimoto, 2021;

Y. Chen et al., 2018; Stadtler et al., 2018; X. Wang et al., 2017; Anderson et al., 2014).

In particular, the evidence for the heterogeneous formation of HONO in relation to high PM_{2.5} and O₃ occurrences in urban areas is increasing (e.g., Y. Li et al., 2021). As an OH reservoir, HONO expedites the photochemical reactions involving VOCs and NO_x in the early morning, leading to O₃ and fine aerosol formation. Nonetheless, its formation mechanism has not been elucidated sufficiently enough to be constrained in conventional photochemical models. In addition to the reaction of NO with OH (Bloss et al., 2021), various pathways of HONO formation have been suggested via laboratory experiments, field measurements, and model simulations: direct emissions from vehicles (S. Li et al., 2021) and soil (Bao et al., 2022); photolysis of particulate nitrate (Gen et al., 2022); and heterogeneous conversion of NO₂ on various aerosol surfaces (Jia et al., 2020), the ground surface (Meng et al., 2022), and microlayers of the sea surface (Gu et al., 2022). Among these, the heterogeneous reaction mechanism on the surface is of major interest.

HONO has been mostly measured during intensive campaigns in urban areas using various techniques and instruments, such as a long path absorption photometer (Xue et al., 2019; Kleffmann et al., 2006), chemical ionization mass spectrometry (Levy et al., 2014; Roberts et al., 2010), ion chromatography (Gil et al., 2020; Xu et al., 2019; Ye et al., 2016; Vandenkoer et al., 2014), a monitor for aerosols and gases in ambient air (MARGA) (Xu et al., 2019), and quantum cascade and tunable infrared laser differential absorption spectrometry (QC-TILDAS) (Gil et al., 2021; Lee et al., 2011). Among these methods, QC-TILDAS has served as a reference for the intercomparison of measurement data obtained using different techniques due to its high time resolution and stability (Pinto et al., 2014). Previous studies have reported that the maximum HONO with levels of several parts per billion (ppb) has been observed at nighttime. In comparison, the WRF-Chem and RACM2 models captured approximately 67%–90% of the observed HONO in megacities such as Beijing (Liu et al., 2019; Tie et al., 2013).

In recent years, machine learning (ML) methods have been employed in the atmospheric science field for pattern classification (e.g., new particle formation event), forecasting, and spatiotemporal modeling of O₃ and PM_{2.5} (Arcomano et al., 2021; Cui and Wang, 2021; Kang et al., 2021; Krishnamurthy et al., 2021; Shahriar et al., 2020; G. Chen et al., 2018; Joutsensaari et al., 2018). Among the ML methods, the neural network (NN) architecture is widely used owing to its powerful ability to process large volumes of data. In particular, a multilayer artificial NN (ANN), referred to as a deep NN (DNN), employs statistical methods to learn nonlinear relationships within the data and yield optimal solutions for a target species without prior knowledge of the underlying physicochemical processes (Schultz et al., 2021; Reichstein et al., 2019). DNN is more beneficial than other NN architectures, such as convolution NN or long short-term memory,

Table 1. Resources for constructing the RND model.

	Version	Remark
Python	v3.8.3	
CUDA	v10.1	*If using GPU
CuDNN	v7.6.5	*If using GPU
TensorFlow	v2.3.0	Python library
Keras	v2.4.3	Python library
Pandas	v1.0.5	Python library
NumPy	v1.18.5	Python library

* GPU signifies graphic processing unit.

because it works well for discrete spatiotemporal data. Generally, the performance of a DNN is similar to or better than that of other ML methods for small and large datasets (Baek and Jung, 2021; Dang et al., 2021; Sumathi and Pugalandhi, 2021).

The DNN method requires lots of data to employ it for atmospheric chemical constituent estimation; therefore, the size of the measurement data is a limiting factor for trace species, such as HONO, that are not routinely measured. In this regard, previous studies have attempted to estimate the daily average HONO mixing ratio by employing ensemble ML models with satellite measurements (Cui and Wang, 2021). Furthermore, a simple NN architecture using ground measurement variables that are believed to be deeply involved in HONO formation was used to calculate the hourly HONO mixing ratio (Gil et al., 2021). The accuracy of the hourly HONO estimated from input variables, such as aerosol surface areas and mixed layer height, is rated better than the daily HONO estimate.

This study aims to develop a user-friendly Reactive Nitrogen Species using a DNN (RNDv1.0) simulation model that estimates the HONO mixing ratios from the real-time measurements of criteria pollutants and meteorological variables. This study is the first to calculate the HONO mixing ratios using RNDv1.0. The entire construction process is comprehensively described, and the performance is evaluated via comparison with the results of simulations using a commonly used model and observations over several years.

2 Model description

The RNDv1.0 development follows systematic steps that are similar to a general ML model construction workflow, including data collection, preprocessing data, building the DNN, training and validating the model, and testing the model performance (Fig. 1). RNDv1.0 is written in Python, and the libraries necessary to build and operate RNDv1.0 are listed in Table 1. The dataset used to train, test, and validate the model can be downloaded from Gil (2021).

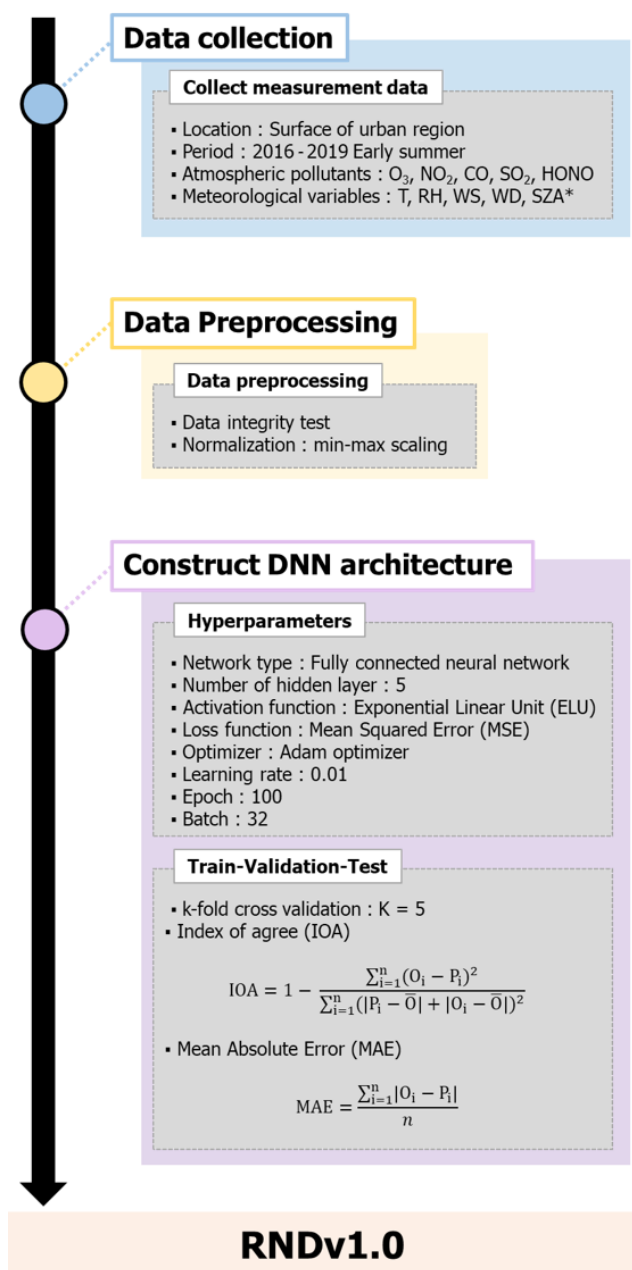


Figure 1. The main processes for configuring RNDv1.0 (* signifies calculated values).

2.1 Collection of measurement data for model construction

To construct RNDv1.0, measurement data were obtained, including HONO, reactive gases, and meteorological variables. Note that the HONO measurement data were used for model construction but are not required to run the RND model. The HONO mixing ratio was measured in Seoul, South Korea, using a QC-TILDAS system during May–June 2016, June 2018, and April–June 2019 (Gil et al., 2021), as well

as a MARGA system during May–June 2021 and October–November 2021 (Gil et al., 2023). When testing and evaluating the atmospheric HONO measurement methods, QC-TILDAS was chosen as the reference method to compare the ambient HONO mixing ratios measured using several different techniques owing to its advantages of having low detection limits (~ 0.1 ppbv) and high temporal resolution (Pinto et al., 2014). More details on measurements can be found elsewhere (Gil et al., 2021).

HONO was measured at the Olympic Park (37.52° N, 127.12° E) during the Korea–United States Air Quality (KORUS-AQ) study in 2016 (Kim et al., 2020; Gil et al., 2021), at the campus of Korea University (37.59° N, 127.03° E) in 2018 and 2021 (Gil et al., 2023), and at another site near the Korea University campus (37.59° N, 127.08° E) in 2019 (NIER, 2020) (Fig. S1). In addition to HONO, trace gases including O₃, NO₂, CO, and SO₂, as well as meteorological variables including temperature (T), relative humidity (RH), wind speed (WS), and wind direction (WD), were measured. Note that HONO was not significantly correlated with any of these variables (Fig. S2). The measurement statistics for the entire experimental periods are presented in Tables 2 and S1. In brief, the 10th and 90th percentile mixing ratios of hourly HONO, NO₂, and O₃ were 0.3 and 2.0 ppbv, 10.0 and 47.0 ppbv, and 8.0 and 75.0 ppbv, respectively.

2.2 Data preprocessing

The observation dataset was prepared for RNDv1.0 model construction. As input variables, hourly measurements of chemical and meteorological variables were used, including the mixing ratios of O₃, NO₂, CO, and SO₂, along with T , RH, WS, WD, and solar zenith angle (SZA), to estimate the target species, HONO, as the output. The WD in degrees was converted to a cosine value for continuity. In the last step of data processing, hourly measurement sets were removed from the input dataset if any of the nine variables was missing. Finally, 54.2 % of all the available measurement data (2847 data points) were used to construct and evaluate RNDv1.0.

Since the measurements of the nine variables considered varied over a wide range of different units, they were normalized to avoid bias during the calculations. Among the widely used normalization methods, the “min–max scaling” method was adopted, and the input variables were normalized against the minimum and maximum values herein (Eq. 1):

$$x_{\text{sca}} = \frac{x_{\text{raw}} - F_2(X)}{F_1(X)}, \quad (1)$$

where x_{raw} is the raw data, x_{sca} is the scaled value, and the scale factors of F_1 and F_2 correspond to the maximum–minimum and minimum values of the input variable (X), respectively, which are listed in Table 2.

Table 2. Input variables and their concentrations (10th–90th percentile of the hourly measurements), coverage, and scale factors for the RNDv1.0 model. Measurements were conducted in Seoul during May–June in 2016 and 2019.

	10th–90th percentile (unit)	Coverage (%)	Scale factor 1 (F_1) ^a	Scale factor 2 (F_2) ^b
Input variables				
O ₃	12.1–90.4 (ppbv)	95.5	204.738	0.842
NO ₂	11.0–48.6 (ppbv)	80.6	79.925	2.375
CO	252–743 (ppbv)	95.1	975.248	137.253
SO ₂	1.9–6.4 (ppbv)	95.6	12.479	0.958
Solar zenith angle	22.7–118.4 (°)	100.0	112.317	14.195
Temperature	15.9–26.7 (° C)	99.4	24.240	8.610
Relative humidity	29.2–79.1 (%)	99.4	88.545	10.555
Wind speed	0.2–3.7 (m s ⁻¹)	99.4	7.581	0.005
Wind direction	45.4–287.5 (°)	99.4	359.565	0.235
Output variables				
HONO	0.3–2.0 (ppbv)	81.1 %	3.447	0.013

^a Maximum–minimum. ^b Minimum value.

2.3 Neural network architecture and hyperparameters

The network was built using the above input variables to calculate HONO. RNDv1.0 comprises five hidden layers (Fig. 2), which employ an exponential linear unit (ELU) as an activation function (Eq. 2).

$$\text{ELU} : \phi(x) = \begin{cases} e^x - 1 & (x < 0) \\ x & (x \geq 0) \end{cases} \quad (2)$$

In a DNN, an activation function creates a nonlinear relationship between an input variable and an output variable. When constructing a DNN model, ELU offers the advantage of a fast training process and exhibits better performance in handling negative values than other activation functions (Ding et al., 2018; T. Wang et al., 2017). Moreover, the mean squared error and Adam optimizer were applied as the loss function and optimization function, respectively. The learning rate, epoch, and batch were set as 0.01, 100, and 32, respectively.

2.4 Model training and k -fold cross validation

RNDv1.0 was trained, validated, and tested with the HONO measurements obtained during May–June 2016 and June 2018, April–June 2019, and May–June 2021 and October–November 2021, respectively (Fig. 3). The number of data used for the training and validation was 1122, and that for testing was 1725.

Using the hyperparameters specified in the previous section, the model performance was first validated using the k -fold cross validation (KFCV) method, which is especially useful for small datasets (Bengio and Grandvalet, 2003). In the KFCV method (Fig. 3), the entire data are randomly divided into k subsets, of which $k - 1$ sets are used for training and the remaining one is used for validation. In this study, k

was set to 5. The accuracy was determined via the index of agreement (IOA), which is expressed as follows (Eq. 3):

$$\text{IOA} = 1 - \frac{\sum_{i=1}^n (O_i - P_i)^2}{\sum_{i=1}^n (|P_i - \bar{O}| + |O_i - \bar{O}|)^2}, \quad (3)$$

where O_i , P_i , \bar{O} , and n are the observed value, predicted value, average of the observed values, and number of nodes, respectively.

As IOA varies according to the number of nodes, it was calculated for the measured (HONO_{obs}) and calculated (HONO_{mod}) mixing ratios by varying the number of nodes from 0 to 100 in each hidden layer. The best performance was obtained with 41 nodes, for which the average IOA was 0.89 ± 0.01 (Fig. 4). The high IOA value signifies that the performance of RNDv1.0 is adequate, and it is capable of simulating the ambient HONO mixing ratio using the routinely measured criteria pollutants and meteorological variables.

The performance of RNDv1.0 was compared with that of other models, including CMAQv5.3.1 (Appel et al., 2021), random forest (RF), and single-layer ANN (Gil et al., 2021), using the 2016 measurement data. The RF model was constructed using the KFCV method and the same input variables as RNDv1.0 (Fig. S4). Its performance was evaluated based on mean absolute error (MAE), root mean square deviation (RMSE), and Pearson correlation coefficient (r):

$$\text{MAE} = \frac{\sum_{i=1}^n |O_i - P_i|}{n}, \quad (4)$$

$$\text{RMSE} = \sqrt{\frac{\sum_{i=1}^n (O_i - P_i)^2}{n}}, \quad (5)$$

$$r = \frac{\text{cov}(O, P)}{\sigma_O \sigma_P}, \quad (6)$$

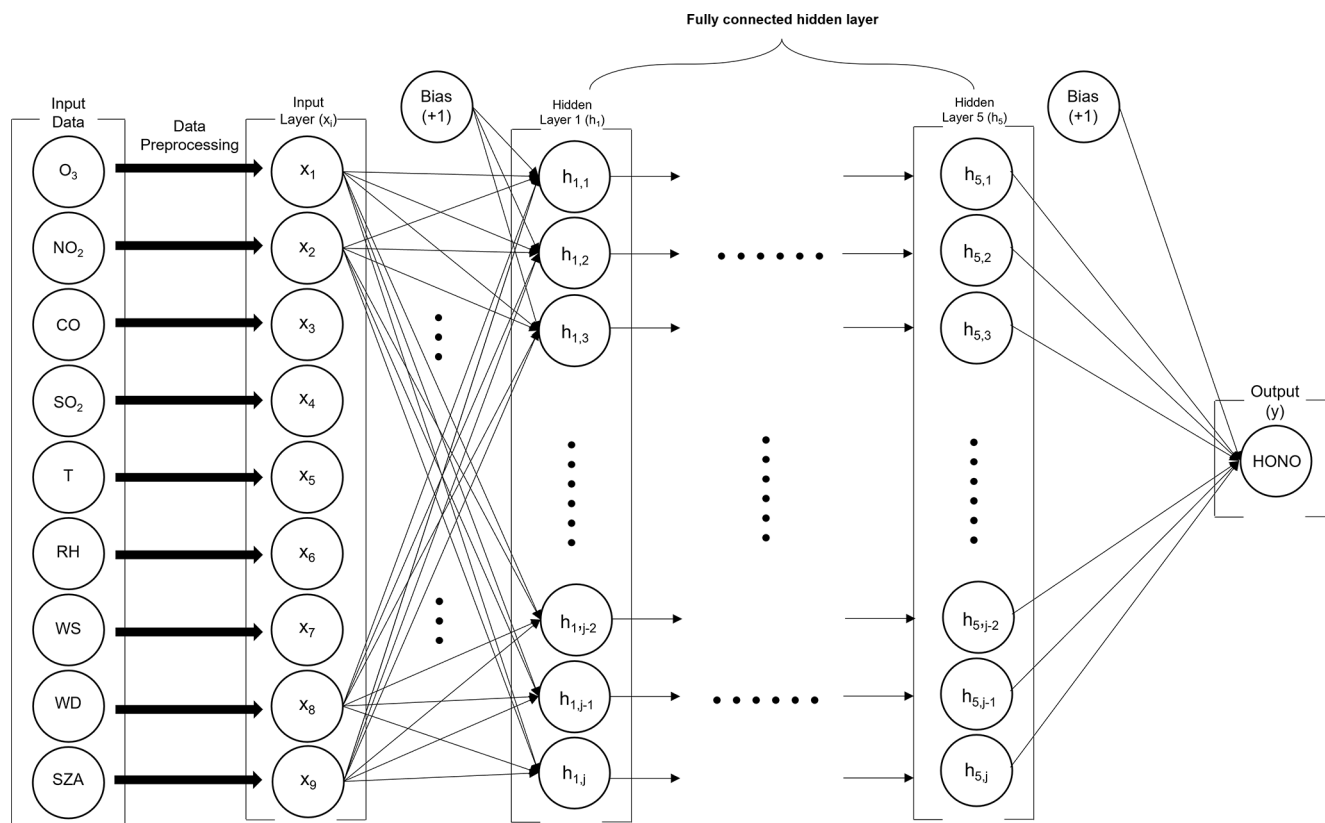


Figure 2. Structure of the deep neural network built for RNDv1.0.

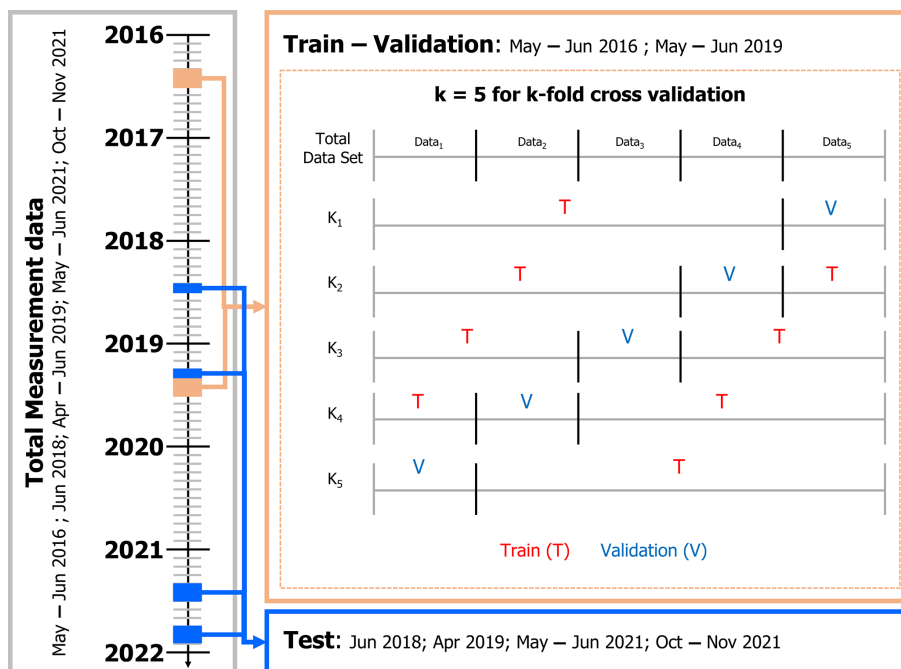


Figure 3. Training, validation, and test design to build RNDv1.0 using the measurement data. The k -fold cross validation was performed using five randomly divided subsets of the training dataset.

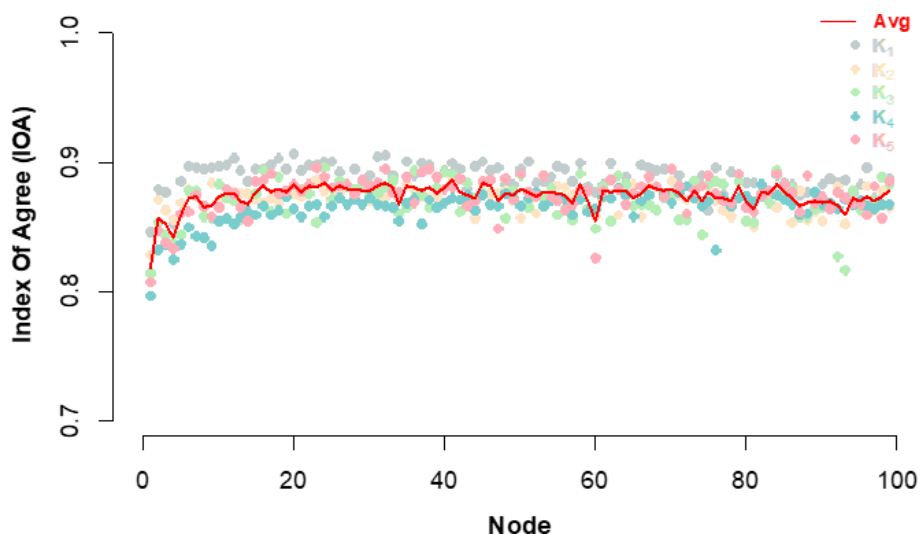


Figure 4. Index of agreement (IOA) for k -fold cross validation. Solid circle and red line represent IOA for each validation ($k = 5$) and the average of five validation sets at each node number.

Table 3. Performance of the chemical transport model (CMAQv5.3.1) and machine learning (ML) models, including random forest (RF), artificial neural network (ANN), and RNDv1.0, on the measurement data from the 2016 KORUS-AQ campaign, which were used for training.

	CMAQv5.3.1	RF	ANN	RNDv1.0
IOA	0.44	0.99	0.86	0.9
r	-0.07	0.99	0.81	0.84
MAE	0.82	0.1	0.38	0.27
RMSE	1.06	0.12	0.41	0.37

where σ and cov denote the standard deviation and covariance, respectively.

All models except CMAQ simulated the measured HONO mixing ratio fairly well (Fig. 5). CMAQ not only underestimated the measured HONO but also failed to represent its diurnal variation (Fig. 6). The statistical information about the performance of the four models is presented in Table 3. The mean measured HONO mixing ratio and those calculated using CMAQ, RF, ANN, and RNDv1.0 were 0.94, 0.09, 0.95, 0.88, and 0.89 ppbv, respectively. Of the four models, RF exhibited the best performance followed by RND. ANN advantageously calculates HONO more accurately than RND as it uses more input variables, but it has a lower data capture rate (41.5 %) compared to RND (97.7 %) or RF (85.3 %).

2.5 Model test

RNDv1.0 and the RF model were tested using data obtained in June 2018, April 2019, May–June 2021, and October–November in 2021, which were not used for RNDv1.0 training (Fig. 3). Note that the RF model outperformed the other

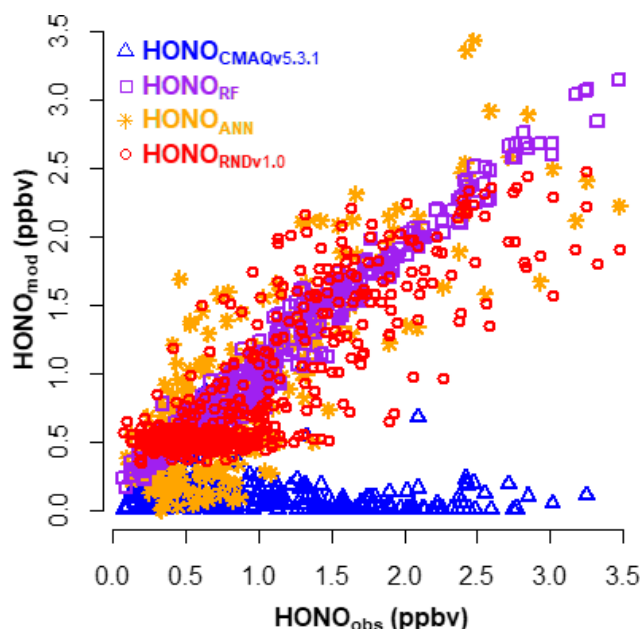


Figure 5. Comparison between the measured HONO (HONO_{obs}) and calculated HONO (HONO_{mod}) using CMAQv5.3.1 (blue triangle), RF (purple square), ANN (orange star), and RNDv1.0 (red circle) during the KORUS-AQ campaign (May–June 2016).

three models in the training and validation process (Fig. 5). Although the performance of RNDv1.0 was slightly lower than that of the RF model, simulated and measured HONO mixing ratios were in good agreement. Interestingly, the performance of the RF model was much worse than RNDv1.0 in the testing process (Fig. 7). The IOA and correlation coefficient of the RF model were extremely low (0.29 and -0.02 , respectively).

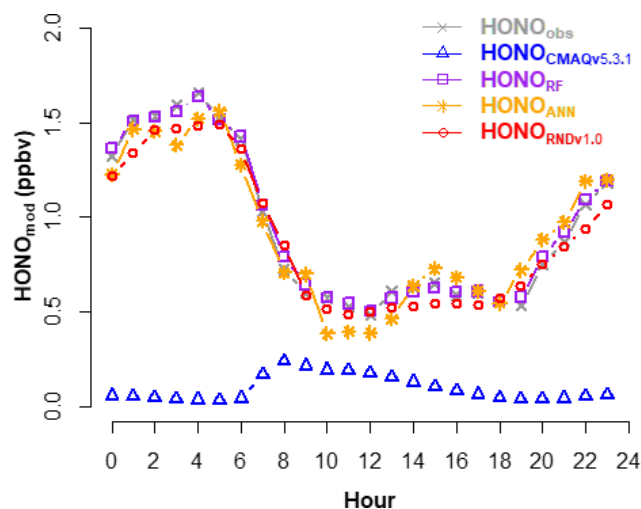


Figure 6. Average diurnal variation in the measured HONO (HONO_{obs}) and calculated HONO (HONO_{mod}) using CMAQv5.3.1 (blue triangle), RF (purple square), ANN (orange star), and RNDv1.0 (red circle) during the KORUS-AQ campaign (May–June 2016).

The performance of RNDv1.0 was slightly lower than that of the RF model, but it traced the HONO mixing ratio well. Among the test dataset, the early winter (October–November) data are particularly valuable for demonstrating the applicability of RNDv1.0 because they stem from different weather conditions than the training dataset. For example, HONO mixing ratios reached over 4 ppbv when the daily average $\text{PM}_{2.5}$ concentration increased to $120 \mu\text{g m}^{-3}$ during severe haze pollution events. Therefore, in the next step, the performance of RNDv1.0 was compared for the two cases by dividing the testing dataset into a group in which all input variables fall within the range of the training dataset and a group which does not meet this criterion. In RNDv1.0, there was no significant difference in performance between the two groups (Fig. S5 and Table S2). When the data in which at least one input variable does not fall within the range of the training dataset were excluded from the test dataset, no significant difference was observed in the performance of RNDv1.0 between the two that meet the same atmospheric conditions or do not meet the criteria (Fig. S5 and Table S2). These extreme atmospheric conditions can worsen the model performance. Except for these extremes, RNDv1.0 traced the variation in the HONO mixing ratio well. These results demonstrate the applicability of RNDv1.0, which is not strictly constrained by atmospheric conditions. The influence of the input variable is further analyzed in the next section.

2.6 Bootstrap test and feature importance

A simple bootstrapping test was conducted for both RNDv1.0 and the RF model to evaluate the relative importance of the input variable to the HONO estimates. In this

analysis, each variable was set to zero, and MAE was calculated as an evaluation metric (Kleinert et al., 2021). Among the nine input variables of RNDv1.0, NO_2 was found to have the greatest influence on HONO concentration, followed by RH and T (Table 4). The highest MAE of 0.59 ppbv could be considered the maximum uncertainty of RNDv1.0 due to the input variable. The bootstrap test result agreed well with that of our previous study (Gil et al., 2021), where more variables such as aerosol surface area and mixing layer height were incorporated into the model, and it highlights the crucial role of precursor gases and heterogeneous conversion in HONO formation.

In contrast, in the RF model, O_3 was the most important variable. This is likely due to the distinct inverse relationship between O_3 and HONO in the diurnal patterns, as well as the O_3 variations over a wide range. In conjunction with the evaluation of the test dataset presented in the previous section, the results of the feature importance for the two models demonstrate the ability of RNDv1.0 to simulate the HONO mixing ratio more adequately in urban areas compared to the RF model. Thus, it is reasonable to state that RNDv1.0 constructed using routinely measured criteria pollutants and meteorological variables can sufficiently capture the HONO variability in the urban atmosphere.

3 Operation and application of RNDv1.0

The RNDv1.0 package is provided as an operational model, and the .h5 files can be opened in Python. To run RNDv1.0, the measurement data for nine input variables are required and need to be properly prepared, as described in Sect. 2.2. Once the input data are ready, open RNDv1.0 with the input data files using the code provided in the example (Fig. S3). Then, RNDv1.0 calculates and presents the HONO results as scaled values (x_{sca}), which then can be converted to the HONO mixing ratio (ppbv) via the two scale factors shown in Table 2 (Eq. 7):

$$\text{HONO (ppbv)} = \text{HONO}_{\text{sca}} \times F_1(\text{HONO}) + F_2(\text{HONO}). \quad (7)$$

The HONO calculated using Eq. (7) can be applied to an urban photochemical cycle simulation. As is already known, the photolysis of HONO is a major source of OH radicals in the early morning when the OH level is low, and this OH affects daytime O_3 formation through photochemical reactions with VOCs and NO_x , which are primarily emitted during the morning rush hour in urban areas. Furthermore, the OH produced from HONO promotes the photochemical oxidation of SO_2 and VOCs, leading to aerosol formation. However, the HONO formation mechanism is still poorly understood, which hinders the accurate simulation of O_3 and fine aerosols, as well as HONO, in conventional photochemical models.

The framework for 0-dimension atmospheric modeling (F0AM), which utilizes the MCM v3.3.1 chemical reac-

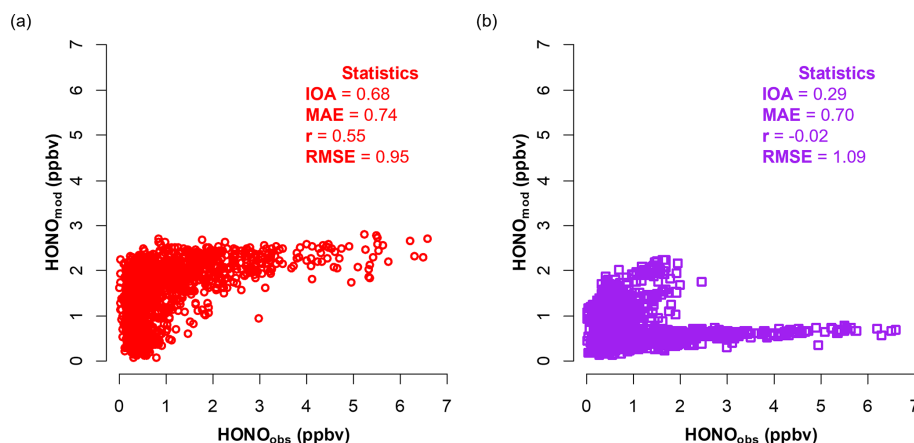


Figure 7. Relationship between measured HONO (HONO_{obs}) and modeled HONO (HONO_{mod}) using (a) RNDv1.0 and (b) a random forest model for the test dataset.

Table 4. Results of the bootstrap test of measurement data used to train the RF and RNDv1.0 models. The greater the MAE, the greater the influence of the variable.

Variable	RF		RNDv1.0	
	MAE	Feature importance	MAE	Feature importance
–	0.10	–	0.28	–
O ₃	0.57	1	0.29	8
NO ₂	0.24	4	0.59	1
CO	0.19	7	0.37	5
SO ₂	0.17	8	0.34	6
Solar zenith Angle (SZA)	0.25	2	0.41	4
Temperature (<i>T</i>)	0.21	5	0.52	2
Relative humidity (RH)	0.25	3	0.52	2
Wind speed (WS)	0.20	6	0.34	6
Wind direction (WD)	0.13	9	0.29	8

tion mechanisms (Wolfe et al., 2016), can be used to simulate the diurnal variation in O₃ with the measurements of several reactive gases (NO, NO₂, CO, HCHO, VOCs, and HONO). Detailed information about F0AM can be found at <https://sites.google.com/site/wolfegm/models> (last access: 6 September 2023) and in previous studies (Gil et al., 2020; Wolfe et al., 2016). When the F0AM model is run without HONO, it is unable to reproduce the concentration and diurnal cycle of the observed O₃ (Fig. 8). In comparison, the model simulates the O₃ well within 2 ppbv when HONO is considered, which is the result of RNDv1.0. This is mainly due to the missing OH produced by HONO photolysis in the early morning. Its production rate is estimated to be 0.57 pptv s⁻¹, contributing approximately 2.28 pptv to the OH budget during 06:00–11:00 (local sun time) (Gil et al., 2021). Given that OH is mainly produced from the photolysis of O₃ under high sun, the early morning supply of OH from HONO photolysis will expedite the photochemical cycle involving NO_x and VOCs, promoting O₃ and secondary aerosol formation. The presence of HONO in the photochem-

ical model allows for the accurate estimation of OH radicals; thus, the incorporation of RNDv1.0 into conventional models will improve their overall performance.

4 Summary and implications

In this study, we developed the RND model to calculate the mixing ratio of NO_y in the urban atmosphere using a DNN along with measurement data. The target species of RNDv1.0 is HONO, and its mixing ratio is calculated using criteria pollutants, including O₃, NO₂, CO, and SO₂, as well as meteorological variables, including *T*, RH, WS, WD, and SZA. These variables are routinely measured through monitoring networks. RNDv1.0 was trained and validated using the HONO measurements data obtained in Seoul by adopting a KFCV method and tested with other HONO datasets. The test results demonstrate that RNDv1.0 adequately captures the characteristic variation in HONO.

RNDv1.0 was constructed using the measurements made in a high-NO_x environment, where the maximum NO₂

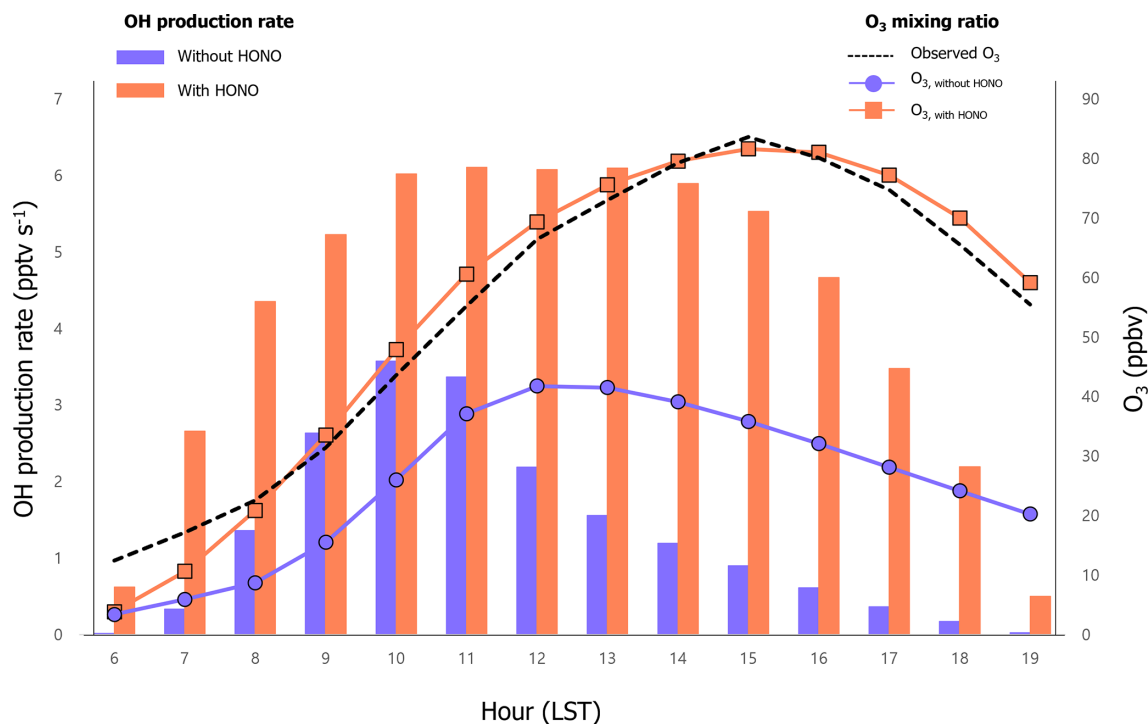


Figure 8. For June 2016, the diurnal variations in O_3 (line) and OH production rate (bar) calculated using the F0AM photochemical model with (orange) and without (blue) HONO estimated from the RNDv1.0 model. The measured and calculated O_3 values are compared.

reached about 80 ppbv. During the measurement period, the HONO mixing ratio was increased up to about 7 ppb under the influence of air masses originating from China. When applying RNDv1.0 to regions or times heavily affected by transport, the model could possibly underestimate the HONO level without more detailed information, such as nanoparticles. Indeed, a previous study showed that HONO formation is closely related to the surface area of particles with diameters in the range of hundreds of nanometers (Gil et al., 2021). Nevertheless, RNDv1.0 is advantageously a relatively inexpensive test for measurement quality control and location selection, and it supports the data used for traditional chemistry models based on the current knowledge of the urban photochemical cycle. Therefore, RNDv1.0 can serve as a supplementary tool for conventional forecasting models. Attempts are currently being made to estimate ground HONO from satellite observations (Armante et al., 2021; Theys et al., 2020; Clarisse et al., 2011), and RNDv1.0 will be useful for validating the satellite-derived HONO.

Code availability. The RND model codes (.h5 files) with preprocessed sample data can be downloaded from <https://doi.org/10.5281/zenodo.5540180> (Gil, 2021).

Data availability. The preprocessed sample data can be downloaded from <https://doi.org/10.5281/zenodo.5540180> (Gil, 2021).

Supplement. The supplement related to this article is available online at: <https://doi.org/10.5194/gmd-16-5251-2023-supplement>.

Author contributions. JG and ML designed the manuscript and developed the model code. JK, GL, and JA provided the HONO measurements, and CHK provided the CMAQ model data. All the authors contributed to the manuscript.

Competing interests. The contact author has declared that none of the authors has any competing interests.

Disclaimer. Publisher's note: Copernicus Publications remains neutral with regard to jurisdictional claims in published maps and institutional affiliations.

Acknowledgements. This study was supported by the National Research Foundation of Korea (2020R1A2C3014592) and the Korea Institute of Science and Technology (KIST2E31650-22-P019).

Financial support. This research has been supported by the National Research Foundation of Korea (grant no. 2020R1A2C3014592) and the Korea Institute of Science and Technology (grant no. KIST2E31650-22-P019).

Review statement. This paper was edited by Leena Järvi and reviewed by four anonymous referees.

References

- Akimoto, H. and Tanimoto, H.: Review of Comprehensive Measurements of Speciated NO_y and its Chemistry: Need for Quantifying the Role of Heterogeneous Processes of HNO₃ and HONO, *Aerosol Air Qual. Res.*, 21, 200395, <https://doi.org/10.4209/aaqr.2020.07.0395>, 2021.
- Akimoto, H., Nagashima, T., Li, J., Fu, J. S., Ji, D., Tan, J., and Wang, Z.: Comparison of surface ozone simulation among selected regional models in MICS-Asia III – effects of chemistry and vertical transport for the causes of difference, *Atmos. Chem. Phys.*, 19, 603–615, <https://doi.org/10.5194/acp-19-603-2019>, 2019.
- Anderson, D. C., Loughner, C. P., Diskin, G., Weinheimer, A., Canty, T. P., Salawitch, R. J., Worden, H. M., Fried, A., Mikoviny, T., and Wisthaler, A.: Measured and modeled CO and NO_y in DISCOVER-AQ: An evaluation of emissions and chemistry over the eastern US, *Atmos. Environ.*, 96, 78–87, 2014.
- Appel, K. W., Bash, J. O., Fahey, K. M., Foley, K. M., Gilliam, R. C., Hogrefe, C., Hutzell, W. T., Kang, D., Mathur, R., Murphy, B. N., Napelenok, S. L., Nolte, C. G., Pleim, J. E., Pouliot, G. A., Pye, H. O. T., Ran, L., Roselle, S. J., Sarwar, G., Schwede, D. B., Sidi, F. I., Spero, T. L., and Wong, D. C.: The Community Multiscale Air Quality (CMAQ) model versions 5.3 and 5.3.1: system updates and evaluation, *Geosci. Model Dev.*, 14, 2867–2897, <https://doi.org/10.5194/gmd-14-2867-2021>, 2021.
- Arcomano, T., Szunyogh, I., Wikner, A., Pathak, J., Hunt, B. R., and Ott, E.: A Hybrid Approach to Atmospheric Modeling that Combines Machine Learning with a Physics-Based Numerical Model, *J. Adv. Model. Earth Sy.*, 14, e2021MS002712, <https://doi.org/10.1029/2021MS002712>, 2021.
- Armante, R., Perrin, A., Kwabia Tchana, F., and Manceron, L.: The ν₄ bands at 11 μm: line lists for the Trans- and Cis-conformer forms of nitrous acid (HONO) in the 2019 version of the GEISA database, *Mol. Phys.*, 120, e1951860, <https://doi.org/10.1080/00268976.2021.1951860>, 2021.
- Arnell, N. W., Lowe, J. A., Challinor, A. J., and Osborn, T. J.: Global and regional impacts of climate change at different levels of global temperature increase, *Climatic Change*, 155, 377–391, 2019.
- Baek, W.-K. and Jung, H.-S.: Performance Comparison of Oil Spill and Ship Classification from X-Band Dual-and Single-Polarized SAR Image Using Support Vector Machine, Random Forest, and Deep Neural Network, *Remote Sens.-Basel*, 13, 3203, <https://doi.org/10.3390/rs13163203>, 2021.
- Bao, F., Cheng, Y., Kuhn, U., Li, G., Wang, W., Kratz, A. M., Weber, J., Weber, B., Pöschl, U., and Su, H.: Key Role of Equilibrium HONO Concentration over Soil in Quantifying Soil–Atmosphere HONO Fluxes, *Environ. Sci. Technol.*, 56, 2204–2212, 2022.
- Bengio, Y. and Grandvalet, Y.: No unbiased estimator of the variance of *K*-fold cross-validation, in: *Advances in Neural Information Processing Systems*, vol. 16, edited by: Thrun, S., Saul, L., and Schölkopf, B., MIT Press, <https://proceedings.neurips.cc/paper/2003/hash/e82c4b19b8151ddc25d4d93baf7b908f-Abstract.html>, last access: 11 September 2003.
- Bloss, W. J., Kramer, L., Crilley, L. R., Vu, T., Harrison, R. M., Shi, Z., Lee, J. D., Squires, F. A., Whalley, L. K., and Slater, E.: Insights into air pollution chemistry and sulphate formation from nitrous acid (HONO) measurements during haze events in Beijing, *Faraday Discuss.*, 226, 223–238, 2021.
- Brown, S. S., An, H., Lee, M., Park, J.-H., Lee, S.-D., Fibiger, D. L., McDuffie, E. E., Dubé, W. P., Wagner, N. L., and Min, K.-E.: Cavity enhanced spectroscopy for measurement of nitrogen oxides in the Anthropocene: results from the Seoul tower during MAPS 2015, *Faraday Discuss.*, 200, 529–557, 2017.
- Canty, T. P., Hembeck, L., Vinciguerra, T. P., Anderson, D. C., Goldberg, D. L., Carpenter, S. F., Allen, D. J., Loughner, C. P., Salawitch, R. J., and Dickerson, R. R.: Ozone and NO_x chemistry in the eastern US: evaluation of CMAQ/CB05 with satellite (OMI) data, *Atmos. Chem. Phys.*, 15, 10965–10982, <https://doi.org/10.5194/acp-15-10965-2015>, 2015.
- Chen, G., Li, S., Knibbs, L. D., Hamm, N. A., Cao, W., Li, T., Guo, J., Ren, H., Abramson, M. J., and Guo, Y.: A machine learning method to estimate PM_{2.5} concentrations across China with remote sensing, meteorological and land use information, *Sci. Total Environ.*, 636, 52–60, 2018.
- Chen, Y., Wolke, R., Ran, L., Birmili, W., Spindler, G., Schröder, W., Su, H., Cheng, Y., Tegen, I., and Wiedensohler, A.: A parameterization of the heterogeneous hydrolysis of N₂O₅ for mass-based aerosol models: improvement of particulate nitrate prediction, *Atmos. Chem. Phys.*, 18, 673–689, <https://doi.org/10.5194/acp-18-673-2018>, 2018.
- Cheng, P., Pour-Biazar, A., White, A. T., and McNider, R. T.: Improvement of summertime surface ozone prediction by assimilating Geostationary Operational Environmental Satellite cloud observations, *Atmos. Environ.*, 268, 118751, <https://doi.org/10.1016/j.atmosenv.2021.118751>, 2022.
- Clarisse, L., R'Honi, Y., Coheur, P. F., Hurtmans, D., and Clerbaux, C.: Thermal infrared nadir observations of 24 atmospheric gases, *Geophys. Res. Lett.*, 38, L10802, <https://doi.org/10.1029/2011GL047271>, 2011.
- Cui, L. and Wang, S.: Mapping the daily nitrous acid (HONO) concentrations across China during 2006–2017 through ensemble machine-learning algorithm, *Sci. Total Environ.*, 785, 147325, <https://doi.org/10.1016/j.scitotenv.2021.147325>, 2021.
- Dang, C., Liu, Y., Yue, H., Qian, J., and Zhu, R.: Autumn crop yield prediction using data-driven approaches: support vector machines, random forest, and deep neural network methods, *Can. J. Remote Sens.*, 47, 162–181, 2021.
- Ding, B., Qian, H., and Zhou, J.: Activation functions and their characteristics in deep neural networks, in: 2018 Chinese Control And Decision Conference (CCDC), Shenyang, China, 9 July 2018, 1836–1841, <https://doi.org/10.1109/CCDC.2018.8407425>, 2018.
- Ge, B., Xu, X., Ma, Z., Pan, X., Wang, Z., Lin, W., Ouyang, B., Xu, D., Lee, J., and Zheng, M.: Role of Ammonia on the Feedback Between AWC and Inorganic Aerosol Formation During Heavy Pollution in the North China Plain, *Astr. Soc. P.*, 6, 1675–1693, 2019.
- Gen, M., Liang, Z., Zhang, R., Mabato, B. R. G., and Chan, C. K.: Particulate nitrate photolysis in the atmo-

- sphere, *Environmental Science: Atmospheres*, 2022, 111–127, <https://doi.org/10.1039/D1EA00087J>, 2022.
- Gil, J.: RNDv1.0 and example, Zenodo [code and data set], <https://doi.org/10.5281/zenodo.5540180>, 2021.
- Gil, J., Son, J., Kang, S., Park, J., Lee, M., Jeon, E., and Shim, M.: HONO measurement in Seoul during Summer 2018 and its Impact on Photochemistry, *Journal of Korean Society for Atmospheric Environment*, 36, 579–588, <https://doi.org/10.5572/KOSAE.2020.36.5.579>, 2020.
- Gil, J., Kim, J., Lee, M., Lee, G., Ahn, J., Lee, D. S., Jung, J., Cho, S., Whitehill, A., Szykman, J., and Lee, J.: Characteristics of HONO and its impact on O₃ formation in the Seoul Metropolitan Area during the Korea-US Air Quality study, *Atmos. Environ.*, 247, 118182, <https://doi.org/10.1016/j.atmosenv.2020.118182>, 2021.
- Gil, J., Lee, M., Lee, H., and Jang, J.: Seasonal Characteristics of HONO Variations in Seoul during 2021–2022, *Journal of Korean Society for Atmospheric Environment*, 39, 308–319, 2023.
- Gu, R., Wang, W., Peng, X., Xia, M., Zhao, M., Zhang, Y., Liu, Y., Shen, H., Xue, L., and Wang, T.: Nitrous acid in the polluted coastal atmosphere of the South China Sea: Ship emissions, budgets, and impacts, *Sci. Total Environ.*, 826, 153692, <https://doi.org/10.1016/j.scitotenv.2022.153692>, 2022.
- IPCC: Summary for policymakers, in: *Climate Change 2014: Impacts, Adaption, and Vulnerability. Part A: Global and Sectoral Aspects. Contribution of Working Group II to the Fifth Assessment Report of the Intergovernmental Panel on Climate Change*, edited by: Field, C. B., Barros, V. R., Dokken, D. J., Mach, K. J., Mastrandrea, M. D., Bilir, T. E., Chatterjee, M., Ebi, K. L., Estrada, Y. O., Genova, R. C., Girma, B., Kissel, E. S., Levy, A. N., MacCracken, S., Mastrandrea, P. R., and White, L. L., Cambridge, United Kingdom and New York, NY, USA, 1–32, <https://doi.org/10.1017/CBO9781107415379.003>, 2014.
- IPCC: Sections, in: *Climate Change 2023: Synthesis Report. Contribution of Working Groups I, II and III to the Sixth Assessment Report of the Intergovernmental Panel on Climate Change*, 35–115, <https://www.ipcc.ch/report/sixth-assessment-report-cycle/>, last access: 11 September 2023.
- Jia, C., Tong, S., Zhang, W., Zhang, X., Li, W., Wang, Z., Wang, L., Liu, Z., Hu, B., and Zhao, P.: Pollution characteristics and potential sources of nitrous acid (HONO) in early autumn 2018 of Beijing, *Sci. Total Environ.*, 735, 139317, <https://doi.org/10.1016/j.scitotenv.2020.139317>, 2020.
- Joutsensaari, J., Ozon, M., Nieminen, T., Mikkonen, S., Lähivaara, T., Decesari, S., Facchini, M. C., Laaksonen, A., and Lehtinen, K. E. J.: Identification of new particle formation events with deep learning, *Atmos. Chem. Phys.*, 18, 9597–9615, <https://doi.org/10.5194/acp-18-9597-2018>, 2018.
- Kang, Y., Choi, H., Im, J., Park, S., Shin, M., Song, C.-K., and Kim, S.: Estimation of surface-level NO₂ and O₃ concentrations using TROPOMI data and machine learning over East Asia, *Environ. Pollut.*, 288, 117711, <https://doi.org/10.1016/j.envpol.2021.117711>, 2021.
- Kim, H., Gil, J., Lee, M., Jung, J., Whitehill, A., Szykman, J., Lee, G., Kim, D.-S., Cho, S., and Ahn, J.-Y.: Factors controlling surface ozone in the Seoul Metropolitan Area during the KORUS-AQ campaign, *Elementa: Science of the Anthropocene*, 8, 46, <https://doi.org/10.1525/elementa.444>, 2020.
- Kleffmann, J., Lörzer, J., Wiesen, P., Kern, C., Trick, S., Volkamer, R., Rodenas, M., and Wirtz, K.: Intercomparison of the DOAS and LOPAP techniques for the detection of nitrous acid (HONO), *Atmos. Environ.*, 40, 3640–3652, 2006.
- Kleinert, F., Leufen, L. H., and Schultz, M. G.: IntelliO3-ts v1.0: a neural network approach to predict near-surface ozone concentrations in Germany, *Geosci. Model Dev.*, 14, 1–25, <https://doi.org/10.5194/gmd-14-1-2021>, 2021.
- Krishnamurthy, R., Newsom, R. K., Berg, L. K., Xiao, H., Ma, P.-L., and Turner, D. D.: On the estimation of boundary layer heights: a machine learning approach, *Atmos. Meas. Tech.*, 14, 4403–4424, <https://doi.org/10.5194/amt-14-4403-2021>, 2021.
- Lee, B. H., Wood, E. C., Zahniser, M. S., McManus, J. B., Nelson, D. D., Herndon, S. C., Santoni, G., Wofsy, S. C., and Munger, J. W.: Simultaneous measurements of atmospheric HONO and NO₂ via absorption spectroscopy using tunable mid-infrared continuous-wave quantum cascade lasers, *Appl. Phys. B*, 102, 417–423, 2011.
- Levy, M., Zhang, R., Zheng, J., Zhang, A. L., Xu, W., Gomez-Hernandez, M., Wang, Y., and Olaguer, E.: Measurements of nitrous acid (HONO) using ion drift-chemical ionization mass spectrometry during the 2009 SHARP field campaign, *Atmos. Environ.*, 94, 231–240, 2014.
- Li, S., Song, W., Zhan, H., Zhang, Y., Zhang, X., Li, W., Tong, S., Pei, C., Wang, Y., and Chen, Y.: Contribution of Vehicle Emission and NO₂ Surface Conversion to Nitrous Acid (HONO) in Urban Environments: Implications from Tests in a Tunnel, *Environ. Sci. Technol.*, 55, 15616–15624, 2021.
- Li, Y., Wang, X., Wu, Z., Li, L., Wang, C., Li, H., Zhang, X., Zhang, Y., Li, J., and Gao, R.: Atmospheric nitrous acid (HONO) in an alternate process of haze pollution and ozone pollution in urban Beijing in summertime: Variations, sources and contribution to atmospheric photochemistry, *Atmos. Res.*, 260, 105689, <https://doi.org/10.1016/j.atmosres.2021.105689>, 2021.
- Li, Z., Xie, P., Hu, R., Wang, D., Jin, H., Chen, H., Lin, C., and Liu, W.: Observations of N₂O₅ and NO₃ at a suburban environment in Yangtze river delta in China: Estimating heterogeneous N₂O₅ uptake coefficients, *J. Environ. Sci.*, 95, 248–255, <https://doi.org/10.1016/j.jes.2020.04.041>, 2020.
- Liebmann, J., Karu, E., Sobanski, N., Schuladen, J., Ehn, M., Schallhart, S., Quéléver, L., Hellen, H., Hakola, H., Hoffmann, T., Williams, J., Fischer, H., Lelieveld, J., and Crowley, J. N.: Direct measurement of NO₃ radical reactivity in a boreal forest, *Atmos. Chem. Phys.*, 18, 3799–3815, <https://doi.org/10.5194/acp-18-3799-2018>, 2018.
- Liu, Y., Lu, K., Li, X., Dong, H., Tan, Z., Wang, H., Zou, Q., Wu, Y., Zeng, L., and Hu, M.: A comprehensive model test of the HONO sources constrained to field measurements at rural North China Plain, *Environ. Sci. Technol.*, 53, 3517–3525, 2019.
- Mallet, V. and Sportisse, B.: Uncertainty in a chemistry-transport model due to physical parameterizations and numerical approximations: An ensemble approach applied to ozone modeling, *J. Geophys. Res.-Atmos.*, 111, D01302, <https://doi.org/10.1029/2005JD006149>, 2006.
- Meng, F., Qin, M., Fang, W., Duan, J., Tang, K., Zhang, H., Shao, D., Liao, Z., Feng, Y., and Huang, Y.: Measurement of HONO flux using the aerodynamic gradient method over an agricultural field in the Huaihe River Basin, China, *J. Environ. Sci.*, 114, 297–307, <https://doi.org/10.1016/j.jes.2021.09.005>, 2022.

- Monks, P. S., Archibald, A. T., Colette, A., Cooper, O., Coyle, M., Derwent, R., Fowler, D., Granier, C., Law, K. S., Mills, G. E., Stevenson, D. S., Tarasova, O., Thouret, V., von Schneidmesser, E., Sommariva, R., Wild, O., and Williams, M. L.: Tropospheric ozone and its precursors from the urban to the global scale from air quality to short-lived climate forcer, *Atmos. Chem. Phys.*, 15, 8889–8973, <https://doi.org/10.5194/acp-15-8889-2015>, 2015.
- Myhre, G., Aas, W., Cherian, R., Collins, W., Faluvegi, G., Flanner, M., Forster, P., Hodnebrog, Ø., Klimont, Z., Lund, M. T., Mülmenstädt, J., Lund Myhre, C., Oliví, D., Prather, M., Quaas, J., Samset, B. H., Schnell, J. L., Schulz, M., Shindell, D., Skeie, R. B., Takemura, T., and Tsyro, S.: Multi-model simulations of aerosol and ozone radiative forcing due to anthropogenic emission changes during the period 1990–2015, *Atmos. Chem. Phys.*, 17, 2709–2720, <https://doi.org/10.5194/acp-17-2709-2017>, 2017.
- NIER: Improvement of Air Quality Forecast based on the Measurement – Focused on Spring Episodes of PM_{2.5}, 1–220, <https://ecolibrary.me.go.kr/nier/#/search/detail/5711273?offset=1> (last access: 11 September 2023), 2020.
- Pinto, J., Dibb, J., Lee, B., Rappenglück, B., Wood, E., Levy, M., Zhang, R. Y., Lefer, B., Ren, X. R., and Stutz, J.: Intercomparison of field measurements of nitrous acid (HONO) during the SHARP campaign, *J. Geophys. Res.-Atmos.*, 119, 5583–5601, 2014.
- Reichstein, M., Camps-Valls, G., Stevens, B., Jung, M., Denzler, J., and Carvalhais, N.: Deep learning and process understanding for data-driven Earth system science, *Nature*, 566, 195–204, 2019.
- Roberts, J. M., Veres, P., Warneke, C., Neuman, J. A., Washenfelder, R. A., Brown, S. S., Baasandorj, M., Burkholder, J. B., Burling, I. R., Johnson, T. J., Yokelson, R. J., and de Gouw, J.: Measurement of HONO, HNCO, and other inorganic acids by negative-ion proton-transfer chemical-ionization mass spectrometry (NI-PT-CIMS): application to biomass burning emissions, *Atmos. Meas. Tech.*, 3, 981–990, <https://doi.org/10.5194/amt-3-981-2010>, 2010.
- Schultz, M., Betancourt, C., Gong, B., Kleinert, F., Langguth, M., Leufen, L., Mozaffari, A., and Stadler, S.: Can deep learning beat numerical weather prediction?, *Philos. T. R. Soc. A*, 379, 20200097, <https://doi.org/10.1098/rsta.2020.0097>, 2021.
- Shahriar, S. A., Kayes, I., Hasan, K., Salam, M. A., and Chowdhury, S.: Applicability of machine learning in modeling of atmospheric particle pollution in Bangladesh, *Air Qual. Atmos. Hlth.*, 13, 1247–1256, 2020.
- Shareef, M. M., Husain, T., and Alharbi, B.: Studying the Effect of Different Gas-Phase Chemical Kinetic Mechanisms on the Formation of Oxidants, Nitrogen Compounds and Ozone in Arid Regions, *Journal of Environmental Protection*, 10, 1006–1031, 2019.
- Shindell, D. T., Lamarque, J.-F., Schulz, M., Flanner, M., Jiao, C., Chin, M., Young, P. J., Lee, Y. H., Rotstayn, L., Mahowald, N., Milly, G., Faluvegi, G., Balkanski, Y., Collins, W. J., Conley, A. J., Dalsoren, S., Easter, R., Ghan, S., Horowitz, L., Liu, X., Myhre, G., Nagashima, T., Naik, V., Rumbold, S. T., Skeie, R., Sudo, K., Szopa, S., Takemura, T., Voulgarakis, A., Yoon, J.-H., and Lo, F.: Radiative forcing in the ACCMIP historical and future climate simulations, *Atmos. Chem. Phys.*, 13, 2939–2974, <https://doi.org/10.5194/acp-13-2939-2013>, 2013.
- Stadler, S., Simpson, D., Schröder, S., Taraborrelli, D., Bott, A., and Schultz, M.: Ozone impacts of gas–aerosol uptake in global chemistry transport models, *Atmos. Chem. Phys.*, 18, 3147–3171, <https://doi.org/10.5194/acp-18-3147-2018>, 2018.
- Stevenson, D. S., Young, P. J., Naik, V., Lamarque, J.-F., Shindell, D. T., Voulgarakis, A., Skeie, R. B., Dalsoren, S. B., Myhre, G., Berntsen, T. K., Folberth, G. A., Rumbold, S. T., Collins, W. J., MacKenzie, I. A., Doherty, R. M., Zeng, G., van Noije, T. P. C., Strunk, A., Bergmann, D., Cameron-Smith, P., Plummer, D. A., Strode, S. A., Horowitz, L., Lee, Y. H., Szopa, S., Sudo, K., Nagashima, T., Josse, B., Cionni, I., Righi, M., Eyring, V., Conley, A., Bowman, K. W., Wild, O., and Archibald, A.: Tropospheric ozone changes, radiative forcing and attribution to emissions in the Atmospheric Chemistry and Climate Model Intercomparison Project (ACCMIP), *Atmos. Chem. Phys.*, 13, 3063–3085, <https://doi.org/10.5194/acp-13-3063-2013>, 2013.
- Sumathi, S. and Pugalendhi, G. K.: Cognition based spam mail text analysis using combined approach of deep neural network classifier and random forest, *J. Amb. Intel. Hum. Comp.*, 12, 5721–5731, 2021.
- Sun, Y., Wang, L., Wang, Y., Quan, L., and Zirui, L.: In situ measurements of SO₂, NO_x, NO_y, and O₃ in Beijing, China during August 2008, *Sci. Total Environ.*, 409, 933–940, 2011.
- Theys, N., Volkamer, R., Müller, J.-F., Zarzana, K. J., Kille, N., Clarisse, L., De Smedt, I., Lerot, C., Finkenzeller, H., and Hendrick, F.: Global nitrous acid emissions and levels of regional oxidants enhanced by wildfires, *Nat. Geosci.*, 13, 681–686, 2020.
- Tie, X., Geng, F., Guenther, A., Cao, J., Greenberg, J., Zhang, R., Apel, E., Li, G., Weinheimer, A., Chen, J., and Cai, C.: Megacity impacts on regional ozone formation: observations and WRF-Chem modeling for the MIRAGE-Shanghai field campaign, *Atmos. Chem. Phys.*, 13, 5655–5669, <https://doi.org/10.5194/acp-13-5655-2013>, 2013.
- VandenBoer, T., Markovic, M., Sanders, J., Ren, X., Pusede, S., Browne, E., Cohen, R., Zhang, L., Thomas, J., and Brune, W. H.: Evidence for a nitrous acid (HONO) reservoir at the ground surface in Bakersfield, CA, during CalNex 2010, *J. Geophys. Res.-Atmos.*, 119, 9093–9106, 2014.
- Varotsos, K., Giannakopoulos, C., and Tombrou, M.: Assessment of the Impacts of climate change on european ozone levels, *Water Air Soil Poll.*, 224, 1596, <https://doi.org/10.1007/s11270-013-1596-z>, 2013.
- Wang, T., Qin, Z., Zhu, M.: An ELU Network with Total Variation for Image Denoising, in: *Neural Information Processing*, edited by: Liu, D., Xie, S., Li, Y., Zhao, D., and El-Alfy, E., ICONIP 2017, Lecture Notes in Computer Science, vol. 10636, Springer, Cham, https://doi.org/10.1007/978-3-319-70090-8_24, 2017.
- Wang, X., Wang, H., Xue, L., Wang, T., Wang, L., Gu, R., Wang, W., Tham, Y. J., Wang, Z., and Yang, L.: Observations of N₂O₅ and ClNO₂ at a polluted urban surface site in North China: High N₂O₅ uptake coefficients and low ClNO₂ product yields, *Atmos. Environ.*, 156, 125–134, 2017.
- Wang, X., Dalton, E. Z., Payne, Z. C., Perrier, S., Riva, M., Raff, J. D., and George, C.: Superoxide and nitrous acid production from nitrate photolysis is enhanced by dissolved aliphatic organic matter, *Environ. Sci. Tech. Let.*, 8, 53–58, 2020.
- Wolfe, G. M., Marvin, M. R., Roberts, S. J., Travis, K. R., and Liao, J.: The Framework for 0-D Atmospheric Modeling (FOAM) v3.1,

- Geosci. Model Dev., 9, 3309–3319, <https://doi.org/10.5194/gmd-9-3309-2016>, 2016.
- Xu, Z., Liu, Y., Nie, W., Sun, P., Chi, X., and Ding, A.: Evaluating the measurement interference of wet rotating-denuder-ion chromatography in measuring atmospheric HONO in a highly polluted area, *Atmos. Meas. Tech.*, 12, 6737–6748, <https://doi.org/10.5194/amt-12-6737-2019>, 2019.
- Xue, C., Ye, C., Ma, Z., Liu, P., Zhang, Y., Zhang, C., Tang, K., Zhang, W., Zhao, X., and Wang, Y.: Development of stripping coil-ion chromatograph method and intercomparison with CEAS and LOPAP to measure atmospheric HONO, *Sci. Total Environ.*, 646, 187–195, 2019.
- Ye, C., Zhou, X., Pu, D., Stutz, J., Festa, J., Spolaor, M., Tsai, C., Cantrell, C., Mauldin, R. L., and Campos, T.: Rapid cycling of reactive nitrogen in the marine boundary layer, *Nature*, 532, 489–491, 2016.